Supporting Information

Tanaka et al. 10.1073/pnas.1015447108

SI Materials and Methods

Generation of *Tdrd7* and *Tdrd6* Gene-Targeted Mice. The *Tdrd7* gene-targeting vector was constructed using a BAC recombineering system (kindly provided by Neal G. Copeland, National Cancer Institute, Bethesda, MD) (1, 2) with BAC clone RP23-190O8 (BACPAC Resource Center). A *LoxP* site was inserted upstream of *Tdrd7* exon 8, and a *pgk-neo* cassette flanked by *FRT* sites and a *loxP* site was targeted downstream of exon 12. For negative selection, a *diphtheria toxin* expression cassette was used. The targeting vector was linearized and electroporated into KY1.1 ES cells (129/B6 F1 hybrid ES cells, kindly provided by Junji Takeda, Osaka University, Osaka, Japan). G418-resistant clones were screened and five clones were identified as having homologously recombined the transgene by PCR and Southern blot analyses. Chimeric mice were produced from two recombinant ES cell clones by aggregation with C57BL/6 × DBA/2 F1 hybrid morulas or by injection into blastocysts. Male chimeras were mated with C57BL/6 females to obtain heterozygous *loxP*-floxed *Tdrd7*-targeted mice. The floxed mice were crossed with *CMV-Cre* transgenic mice (C57BL/6 strain) (3) to excise *loxP*-flanked exons 8–12. *Tdrd7* homozygous null mice were obtained by intercrossing *Tdrd7* heterozygous mice, and generations between 2 and 15 were used for the analyses in this study. The *Tdrd6* gene-targeting vector was constructed using the BAC recombineering system with BAC clone RP23-283P8. The 2.6-kb genomic region in the first exon (NM_198418, 99–2698) was replaced with a neomycin resistance gene. The targeting vector had a *diphtheria toxin* expression cassette for negative selection. The vector was linearized and electroporated into V6.5 ES cells (129/B6 F1 hybrid ES cells, kindly provided by Rudolf Jaenisch, Whitehead Institute, Massachusetts Institute of Technology, Cambridge, MA) (4). G418-resistant clones were screened by PCR and Southern blot analyses, and 10 clones were identified as having homologously recombined the transgene. Chimeric mice were produced from two recombinant ES cell clones by aggregation with C57BL/6 × DBA/2 F1 hybrid morulas or by injection into blastocysts. Male chimeras were mated with C57BL/6 females to obtain heterozygous *Tdrd6* gene-targeted mice. Homozygous targeted mice were obtained by intercrossing heterozygous mutant mice. All of the animal experiments were performed according to our institution's ethical guidelines.

Southern Blots. Tail genomic DNA (10 μg) was digested with restriction enzymes, electrophoresed by using an 0.8% agarose gel, and transferred onto a nylon membrane (Hybond-XL, GE). The blot was hybridized with a [α-^{32}P]dCTP-labeled genomic fragment of *Tdrd7* and *Tdrd6*, which was PCR-amplified with the primers 5′-AGAACAAGAGAAGACCTCTCCTGG-3′ and 5′-CCTCAAAGCTAAGGAACCATGC-3′ and 5′-AAACTGAAACCCAGAGAAAGGAGGG-3′ and 5′-CCAGGCAAATCACCCACACATGTCA-3′, respectively. Signals were detected by using X-ray film (Kodak).

RT-PCR and Northern Blots. Total RNA was extracted from tissues using the acid guanidinium phenol chloroform (AGPC) method (TRIzol, Invitrogen). For RT-PCR, 1 μg of RNA was treated with DNase I (Promega), reverse-transcribed, and used as a PCR template (High Capacity RNA-to-cDNA kit, Applied Biosystems). Quantitative RT-PCR was performed using ABI PRISM 7700 with SYBR Green PCR Master Mix (Applied Biosystems). Relative mRNA levels were determined from threshold cycles for amplification using the ΔΔCt method. β-Actin was used for normalization and fold changes between mutants, and controls were calculated. The assays were done in triplicate wells. The primers used for *LINE1* are 5′-GGCGAAAGGCAAACGTAAGA-3 and 5′-GGAGTGCTGCGTTCTGATGA-3′, which amplify the 5′ end of ORF1 (5). Other primer sequences used are available on request. For Northern blotting, 15 μg of total RNA was separated on a 1% formaldehyde agarose gel, transferred to nylon membrane (Hybond N+, GE), and probed with a 4.2-kb fragment of *LINE1* 5′ UTR (6) labeled with [α-^{32}P]dCTP. Signals were detected by using X-ray film (Kodak).

Western Blots. Tissue/cell lysates were subjected to 5–20% gradient SDS/PAGE and transferred onto nitrocellulose membranes (Protran BA, Schleicher & Schuell). The blots were probed with primary antibodies followed by alkaline phosphatase-conjugated secondary antibodies (Dako). The primary antibodies against TDRD1, -6, -7 (7, 8), and LINE1 ORF1 protein (kindly provided by Sandra L. Martin) (9) are as described previously. Anti-MILI (Abcam), DDX6 (Bethyl), RPS6 (Novus), SYCP1, GAPDH (Chemicon), β-actin (Sigma), and SYCP3 (10) antibodies were also used. Signals were detected by using CDP-Star with NitroBlock II (Perkin-Elmer) and X-ray film.

Histological and Immunohistological Examination. For histology, tissues were fixed in Bouin's solution, embedded in paraffin wax, cut into 7-μm thick sections, and then stained with hematoxylin and eosin dyes. For immunofluorescence staining, tissues fixed with 2% paraformaldehyde (PFA) in PBS were cryo-embedded in optimal cutting temperature (OCT) compound (Sakura) and cut into 10-μm thick sections. Antibodies against TDRD1, -6, -7, and -9 (7, 8); MIWI2 (5); SYCP3 (10); LINE1 ORF1 protein (kindly provided by Sandra L. Martin, University of Colorado School of Medicine, Denver, CO) (9); GENA (kindly provided by Yoshitake Nishimune, Osaka University, Osaka, Japan) (11); TNP1 and -2 (kindly provided by W. Stephen Kistler, University of South Carolina, Columbia, SC) (12, 13); PRM1 and -2 (kindly provided by Rod Balhorn, Lawrence Livermore National Laboratory, Livermore, CA) (14, 15); and LAMP2 (ABL-93, Developmental Studies Hybridoma Bank) (16) are as described previously. Anti-MVH, MILI, PABPC1 (Abcam), Ub (MBL), MIWI, EIF4E (Cell Signaling), TIAR, EEA1, AP-α, GM130 (BD), LC3 (Abgent), AGO2 (Abnova), anti–phospho-histone H2A.X (Upstate, Millipore), and DDX6 (Bethyl) antibodies were also used. The secondary antibodies were Alexa 488 or Alexa 568-conjugated anti-rat, rabbit, and mouse IgGs (Invitrogen). Antigen retrieval for TDRD9 and DDX6 staining was carried out by autoclaving Bouin's-fixed paraffin sections at 120 °C for 15 min in 10 mM Tris–Cl (pH 9.0), 1 mM EDTA, and 0.01% Tween20. For anti-TNP1 and PRM1 detection, antigen retrieval was carried out by incubating 2% PFA-fixed paraffin sections at 90 °C for 20 min in sodium citrate buffer (pH 6.0). Apoptotic cells were detected by using the TUNEL method (In Situ Cell Death Detection Kit, Roche). Nuclei were counterstained with 1 μg/mL Hoechst 33258 dye (Sigma).

Electron and Immunoelectron Microscopy. Testes were fixed with 2% glutaraldehyde in 0.1 M phosphate buffer (pH 7.2), postfixed with 1% OsO4 and 0.1 M sucrose in 0.1 M phosphate buffer, dehydrated with graded concentrations of ethanol and then embedded in epoxy resin. Semithin 1-μm sections were stained with 0.1% toluidine blue for light microscopy. Sections (70–90 nm) were placed on 150-mesh copper grids, stained with uranyl acetate

followed by lead citrate, and then examined by using an electron microscope (H7700, Hitachi). For immunoelectron microscopy of MVH and MIWI, immunoelectron microscopy was performed as reported previously (8). In brief, testes were fixed in 2% PFA and 0.02% glutaraldehyde in 0.1 M phosphate buffer (pH 7.4) and embedded in epoxy resin. Sections of 90 nm were incubated with anti-MVH (Abcam) or with anti-MIWI (Cell Signaling) antibodies, followed by 15-nm gold-labeled secondary antibody [AuroProbe EM anti-rabbit IgG (HCL) and 15 nm gold (GE Healthcare)]. After postfixation with 2% glutaraldehyde in PBS, the sections were stained with uranylacetate and lead citrate and examined by using an electron microscope (H-7650, Hitachi).

RNA in Situ Hybridization. Testes were fixed in 4% PFA in PBS and embedded in OCT compound (Sakura), and 8-μm sections were cut. Sense and antisense digoxigenin (DIG)-labeled (Roche) RNA probes were transcribed from a linearized plasmid (pCRII-TOPO, Invitrogen) containing *Tnp2* (NM_013694, 1–490). For oligo dT and dA probes, oligo(dT)20 and oligo(dA)20 oligodeoxynucleotides were end-labeled with DIG (DIG-Oligonucleotide 3′-End Labeling Kit, Roche). Signals were detected using horseradish peroxidase-conjugated anti-DIG antibody (Dako), biotinyl tyramide (Perkin-Elmer), and FITC-conjugated streptavidin (Dako). Nuclei were counterstained with 1 μg/mL Hoechst 33258 dye (Sigma). For electron microscopy, a post-embedding technique was used as described previously (17). Briefly, testes were fixed in 4% PFA and 1% glutaraldehyde in 0.1 M phosphate buffer (pH 7.4), dehydrated, embedded in London Resin (LR) white resin (NEM), and then cut into 70- to 90-nm sections. The sections were then hybridized with DIG-labeled RNA or oligo probes as described above. Detection was carried out by using sheep anti-DIG antibody (Dako), followed by 20- or 40-nm gold particle-conjugated anti-sheep IgGs (Jackson Laboratory). The sections were stained with uranyl acetate and lead citrate and then examined using an H-7650 electron microscope.

DNA Methylation Analysis. For methylation-sensitive Southern blotting, 10 μg of genomic DNAs from testes were digested with methylation-sensitive HpaII or methylation-insensitive MspI, resolved in an 0.8% agarose gel and transferred onto nylon membranes (Hybond-XL, GE). The blots were hybridized with [α-^{32}P]dCTP-labeled probe of *LINE-1* 5′-UTR (type A) (6). Bisulfite sequencing was carried out as described (18). Primers used were 5′-caggatcctaggaaattagtttgaataggtgagagggt-3′ and 5′-gtaagcttccaaaacaaaaccttctcaaacactatat-3′ (type Tf) (19). The amplified products were subcloned into pBluescript SK and sequenced. Germ cells were isolated from *Tdrd7*$^{+/-}$ and $^{-/-}$ testes by FACS as previously described (18). Briefly, single-cell suspensions from testes were obtained by collagenase and trypsin digestion, and the cells were fixed with 4% PFA in PBS (−), permeabilized with 0.1% TritonX-100 in PBS (−), and then immunostained with anti-TRA98/104 antibody (11), followed by Alexa 546-conjugated anti-rat IgG (Invitrogen). FACS-sorted cells were treated with proteinase K (200 μg/mL) at 55 °C overnight, and genomic DNAs were extracted and analyzed by bisulfite sequencing as described above.

Microarray Analysis. For the microarray analysis, spematids were enriched from single-cell suspensions of *Tdrd7*$^{+/-}$ and *Tdrd7*$^{-/-}$ testes that were dissociated with collagenase and trypsin digestion and separated by centrifugal elutriation (R5E, Hitachi) (20). Total RNAs were extracted using the AGPC method (TRIzol, Invitrogen) and biotinylated cRNA probes were amplified using an Illumina TotalPrep RNA Amplification Kit (Ambion). MouseWG-6 Expression Beadchips (Illumina) were hybridized and scanned according to the manufacturer's instruction. Data with detection *P*-values of > 0.01 were used for differential expression analyses.

Immunoprecipitation. RNA immunoprecipitation was carried out as described (21). Briefly, single-cell suspensions from testes were fixed by 0.1% formaldehyde for 10 min at room temperature. After addition of 0.25 M glycine for 5 min, cells were harvested and lysed with RIPA buffer (50 mM Tris·HCl pH 7.4, 1% Nonidet P-40, 0.5% Na deoxycholate, 0.05% SDS, 1 mM EDTA, and 150 mM NaCl) followed by sonication. After centrifugation, lysates were precleared with protein G-coupled magnetic beads (Invitrogen) and used for immunoprecipitation for 4 h at 4 °C. Immunoprecipitation was carried out with magnetic beads coupled with anti-TDRD7, anti-EIF4E, and anti-PABP antibodies or normal rabbit IgG as a control (Santa Cruz). The RNAs in the immunoprecipitates were reverse-crosslinked with SDS and Proteinase K at 65 °C for 1 h, extracted using the AGPC method, and then analyzed by real-time RT-PCR as described.

Sucrose Gradient Polysome Fractionation. Testicular extracts from *Tdrd7*$^{+/-}$ and *Tdrd7*$^{-/-}$ mice (P22) were subjected to sucrose gradient fractionation as described previously (22). Briefly, testicular lysates [20 mM Tris–Cl (pH 7.4), 150 mM KCl, 5 mM MgCl2, 2 mM DTT, 0.5% Nonidet P-40] were centrifuged at 1,000 × *g* at 4 °C for 10 min, and the supernatant was applied to the top of a 15–50% linear sucrose gradient. Cycloheximide (100 μg/mL) was added to stabilize polysomes (in the absence of puromycin). Puromycin was added to a final concentration of 200 μg/mL [20 mM Tris–Cl (pH 7.4) 500 mM KCl, 2 mM DTT, 0.5% Nonidet P-40]. The gradient was centrifuged at 150,000 × *g* for 3 h (Hitachi). Twenty-eight fractions (0.3 mL) were collected, and the RNAs were extracted using the AGPC method, treated by DNaseI, and reverse-transcribed as described above. Relative abundance of LINE1 and β-actin RNA was measured by real-time RT-PCR. Proteins were separated by SDS/PAGE, and Western blots were probed with rabbit anti-RPS6 and anti-MILI antibodies as described above.

Protein Stability Analysis. Single-cell suspensions from *Tdrd7*$^{+/-}$ and $^{-/-}$ testes (3 wk) were obtained by collagenase and trypsin digestion, and then the cells were resuspended in Dulbecco's Modified Eagle's Medium/Nutrient F-12 Ham medium supplemented with 10% FBS. Cycloheximide, a translation inhibitor, was added to a final concentration of 100 μg/mL and the cells were cultured at 34 °C with 5% CO_2. Equal numbers of cells were collected at 0, 3, and 6 h and then subjected to Western blot analysis. To avoid saturation of autoradiography of LINE1 ORF1 in *Tdrd7*$^{-/-}$ samples, a 1:10 dilution of the cell lysate was loaded for *Tdrd7*$^{-/-}$ samples and used for relative quantification.

RNA Transcription and Stability Analysis. Relative transcription was measured by metabolic labeling using the Click-iT Nascent RNA capture kit (Invitrogen) according to the manufacturer's instruction. Briefly, single-cell suspensions from *Tdrd7*$^{+/-}$ and *Tdrd7*$^{-/-}$ testes (3 wk) were prepared as described above and then cultured for 1 h in the presence of uridine analog 5-ethynyluridine (EU) at a final concentration of 1 mM, which was incorporated into newly transcribed RNA. Total RNAs were extracted by using the TRIzol reagent and then used in a copper-catalyzed click reaction with an azide–biotin, which creates biotinylated RNA. The biotin nascent transcripts were captured on streptavidin magnetic beads and then used for cDNA synthesis. Quantitative RT-PCR was performed by using StepOnePlus real-time PCR system and SYBR Green PCR Master Mix (Applied Biosystems). Relative transcript levels were determined from threshold cycles for amplification using the ΔΔCt method from triplicate wells. *18S rRNA* was used for normalization. Data were obtained from

four independent experiments. Before analyzing the *LINE1* transcription in *Tdrd7*$^{-/-}$ samples, we evaluated the validity of this method for testicular cells by measuring the retinoic acid response, which is a well-established model of transcriptional regulation. In the presence of retinoic acid, the transcription levels of *RARβ* and *Stra8*, both of which are direct targets of the retinoic acid pathway, were clearly up-regulated when examined by the EU metabolic labeling experiment (data available upon request), confirming that this method is useful to analyze relative transcription in spermatogenic cells.

To analyze RNA stability, single-cell suspensions from *Tdrd7*$^{+/-}$ and *Tdrd7*$^{-/-}$ testes (3 wk) were cultured in the presence of 1 mM of 5,6-dichlorobenzimidazole (DRB), which inhibits RNA polymerase II by causing premature termination of transcription. Samples were collected at 0, 3, and 6 h. RNA extraction, reverse transcription, and quantitative PCR were carried out as described. The pan-caspase inhibitor Z-VAD-FMK was used to suppress apoptosis in these culture experiments.

Piwi-Interacting RNA (piRNA) Sequence Analysis. Deep sequence analysis of piRNAs was carried as described (18, 23). Briefly, after clipping the linker sequence, piRNA sequences were mapped to the mouse genome (release mm8) and then used for further analysis. Annotation categories were assigned on the basis of the annotation of corresponding genomic sequences extracted from the University of California at Santa Cruz genome browser. Nucleotide biases were calculated for piRNAs matching *LINE1* consensuses. To extract piRNA clusters, the genome was scanned using a 10-kb window. To identify sequences that match the consensuses for transposable elements, piRNAs were aligned to consensus sequences from the Repbase release (http://www.girinst.org/). L1_MM (GenBank M29324) was used for *LINE1*. The analysis was carried out using "the small RNA dashboard" application server (http://katahdin.mssm.edu/html/scripts/resources.pl). The sequence reads (after the genome mapping) were 2,387,787 for *Tdrd7*$^{+/-}$ 18d; 3,038,408 for *Tdrd7*$^{-/-}$ 18d; 2,646,993 for *Tdrd7*$^{+/-}$ 6w; and 2,574,308 for *Tdrd7*$^{-/-}$ 6w.

Primary Culture of Testicular Cells. Single-cell suspensions from wild-type testes were obtained by collagenase and trypsin digestion, and then the cells were resuspended in Dulbecco's Modified Eagle's Medium/Nutrient F-12 Ham medium supplemented with 10% FBS. 5′-Methylthioadenosine (MTA), a methyltransferase inhibitor, was added to a final concentration of 500 μM and the cells were cultured at 32 °C with 5% CO_2. Cultured cells were collected at 3 and 6 h and then subjected to immunostaining with anti-TDRD6, anti-TDRD7, and anti-SYCP3 antibodies. Nuclei were counterstained with 1 μg/mL Hoechst 33258 dye (Sigma).

1. Lee EC, et al. (2001) A highly efficient Escherichia coli-based chromosome engineering system adapted for recombinogenic targeting and subcloning of BAC DNA. *Genomics* 73:56–65.
2. Liu P, Jenkins NA, Copeland NG (2003) A highly efficient recombineering-based method for generating conditional knockout mutations. *Genome Res* 13:476–484.
3. Dupé V, et al. (1997) In vivo functional analysis of the Hoxa-1 3′ retinoic acid response element (3′RARE). *Development* 124:399–410.
4. Eggan K, et al. (2001) Hybrid vigor, fetal overgrowth, and viability of mice derived by nuclear cloning and tetraploid embryo complementation. *Proc Natl Acad Sci USA* 98: 6209–6214.
5. Carmell MA, et al. (2007) MIWI2 is essential for spermatogenesis and repression of transposons in the mouse male germline. *Dev Cell* 12:503–514.
6. Bourc'his D, Bestor TH (2004) Meiotic catastrophe and retrotransposon reactivation in male germ cells lacking Dnmt3L. *Nature* 431:96–99.
7. Hosokawa M, et al. (2007) Tudor-related proteins TDRD1/MTR-1, TDRD6 and TDRD7/TRAP: domain composition, intracellular localization, and function in male germ cells in mice. *Dev Biol* 301:38–52.
8. Chuma S, et al. (2006) Tdrd1/Mtr-1, a tudor-related gene, is essential for male germ-cell differentiation and nuage/germinal granule formation in mice. *Proc Natl Acad Sci USA* 103:15894–15899.
9. Branciforte D, Martin SL (1994) Developmental and cell type specificity of LINE-1 expression in mouse testis: Implications for transposition. *Mol Cell Biol* 14:2584–2592.
10. Chuma S, Nakatsuji N (2001) Autonomous transition into meiosis of mouse fetal germ cells in vitro and its inhibition by gp130-mediated signaling. *Dev Biol* 229:468–479.
11. Tanaka H, et al. (1997) A germ cell-specific nuclear antigen recognized by a monoclonal antibody raised against mouse testicular germ cells. *Int J Androl* 20: 361–366.
12. Heidaran MA, Showman RM, Kistler WS (1988) A cytochemical study of the transcriptional and translational regulation of nuclear transition protein 1 (TP1), a major chromosomal protein of mammalian spermatids. *J Cell Biol* 106:1427–1433.
13. Alfonso PJ, Kistler WS (1993) Immunohistochemical localization of spermatid nuclear transition protein 2 in the testes of rats and mice. *Biol Reprod* 48:522–529.
14. Stanker LH, Wyrobek A, Balhorn R (1987) Monoclonal antibodies to human protamines. *Hybridoma* 6:293–303.
15. Stanker LH, et al. (1992) Immunological evidence for a P2 protamine precursor in mature rat sperm. *Mol Reprod Dev* 33:481–488.
16. Moreno RD (2003) Differential expression of lysosomal associated membrane protein (LAMP-1) during mammalian spermiogenesis. *Mol Reprod Dev* 66:202–209.
17. Gomez E, et al. (1997) Type I and type II interleukin-1 receptor expression in rat, mouse, and human testes. *Biol Reprod* 56:1513–1526.
18. Shoji M, et al. (2009) The TDRD9-MIWI2 complex is essential for piRNA-mediated retrotransposon silencing in the mouse male germline. *Dev Cell* 17:775–787.
19. Kato Y, et al. (2007) Role of the Dnmt3 family in de novo methylation of imprinted and repetitive sequences during male germ cell development in the mouse. *Hum Mol Genet* 16:2272–2280.
20. Meistrich ML, Longtin J, Brock WA, Grimes SR Jr., Mace ML (1981) Purification of rat spermatogenic cells and preliminary biochemical analysis of these cells. *Biol Reprod* 25:1065–1077.
21. Kaneko S, Manley JL (2005) The mammalian RNA polymerase II C-terminal domain interacts with RNA to suppress transcription-coupled 3′ end formation. *Mol Cell* 20: 91–103.
22. Grivna ST, Pyhtila B, Lin H (2006) MIWI associates with translational machinery and PIWI-interacting RNAs (piRNAs) in regulating spermatogenesis. *Proc Natl Acad Sci USA* 103:13415–13420.
23. Aravin AA, Sachidanandam R, Girard A, Fejes-Toth K, Hannon GJ (2007) Developmentally regulated piRNA clusters implicate MILI in transposon control. *Science* 316: 744–747.

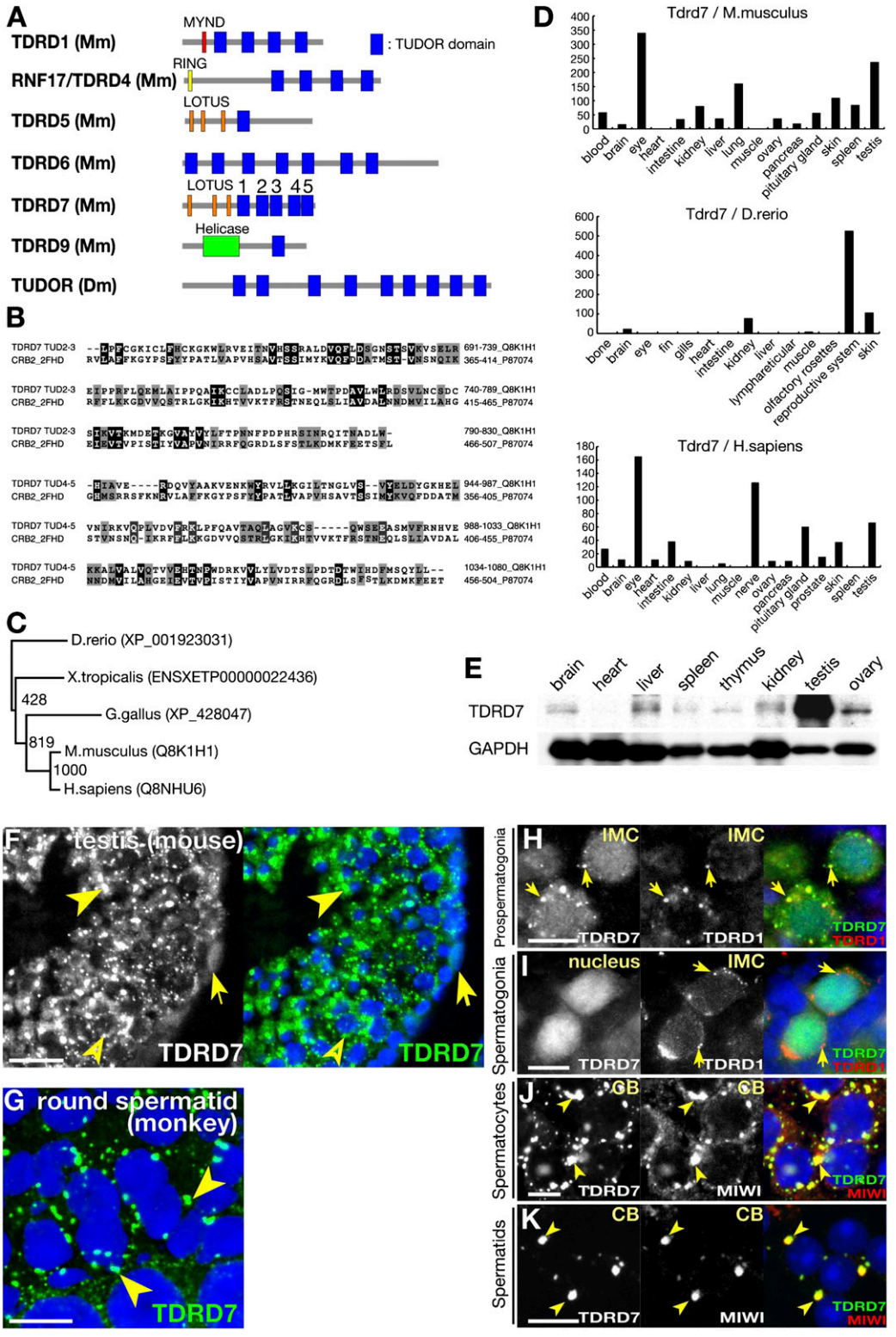

Fig. S1. TDRD7 is a conserved component of mammalian germinal granules. (*A*) Domain architecture of selected tudor proteins, mouse TDRD1, RNF17/TDRD4, TDRD5, TDRD6, TDRD7, TDRD9, and *Drosophila* TUDOR (1–6). The blue boxes represent tudor domains, and the red, yellow, orange, and green boxes are MYND, RING, LOTUS, and DExH helicase domains, respectively. Three putative LOTUS domains with unknown function were predicted in the N-terminal region of TDRD7 (7, 8). (*B*) Sequence alignment of TDRD7 with a tandem Tudor domain sequence of yeast CRB2 protein (9) by ClustalW. Identical and similar residues are in reverse and shaded fonts, respectively. (*C*) Phylogenetic tree of TDRD7 amino acid sequences obtained from the RefSeq database (National Center for Biotechnology Information, accession numbers in parentheses; XP denotes hypothetical proteins). Multiple alignment was carried out by using ClustalW with bootstrapping (n = 1,000) and without an out-group. The bootstrap values are shown at the nodes. (*D*) EST profiles of *Mus musculus*, *Danio rerio*, and *Homo sapiens Tdrd7* from the UniGene database (National Center for Biotechnology Information). The values are transcripts per million. *Tdrd7* transcripts were abundant in reproductive organs as well as in several somatic tissues, including the eye and nervous system. This contrasted with other *Tdrd* genes, including

Legend continued on following page

Tdrd1, *-2*, *-4*, *-5*, *-6*, and *-9*, which are more preferentially expressed in the testis and/or ovary (2–6, 10, 11). (*E*) Western blots of selected mouse tissues with anti-TDRD7 and control anti-GAPDH antibodies. The TDRD7 protein was most abundantly detected in the testis. (*F*) A section of a mouse testis immunostained with anti-TDRD7 (green) and counterstained with a Hoechst dye (blue). The arrow, open arrowhead, and arrowhead indicate a spermatogonia, spermatocyte, and spermatid, respectively. (*G*) A section of a monkey testis (*Macaca fascicularis*) immunostained with anti-TDRD7 (green) counterstained with a Hoechst dye (blue). The arrowheads indicate chromatoid bodies. (*H–K*) Double immunostain of fetal prospermatogonia at embryonic day 17.5 (*H*) and postnatal spermatogonia (*I*), meiotic spermatocytes (*J*), and haploid round spermatids (*K*) with anti-TDRD7 (green), TDRD1 (marker of intermitochondrial cement: *H* and *I*, red), and MIWI (marker of chromatoid body: *J* and *K*, red) antibodies. The arrows indicate intermitochondrial cement (IMC) and the arrowheads mark chromatoid bodies (CB). In fetal prospermatogonia (*H*), TDRD7 was enriched at intermitochondrial cement in the cytoplasm. Subsequently, in postnatal spermatogonia (*I*) and early meiotic spermatocytes (at the leptotene–zygotene stages), TDRD7 was translocated into the nucleus. Then in mid-to-late spermatocytes (at the pachytene stage: *J*) and haploid spermatids (*K*), when chromatoid bodies emerge, TDRD7 was clearly localized at chromatoid bodies. TDRD7 at these stages also shows smaller cytoplasmic granules, the identi is still unclear. (Scale bars: *F*, 25 μm; *G–K*, 10 μm.)

1. Thomson T, Lasko P (2004) Drosophila tudor is essential for polar granule assembly and pole cell specification, but not for posterior patterning. *Genesis* 40:164–170.
2. Hosokawa M, et al. (2007) Tudor-related proteins TDRD1/MTR-1, TDRD6 and TDRD7/TRAP: Domain composition, intracellular localization, and function in male germ cells in mice. *Dev Biol* 301:38–52.
3. Pan J, et al. (2005) RNF17, a component of the mammalian germ cell nuage, is essential for spermiogenesis. *Development* 132:4029–4039.
4. Yabuta Y, et al. (2011) TDRD5 is required for retrotransposon silencing, chromatoid body assembly, and spermiogenesis in mice. *J Cell Biol* 192:781–795.
5. Shoji M, et al. (2009) The TDRD9-MIWI2 complex is essential for piRNA-mediated retrotransposon silencing in the mouse male germline. *Dev Cell* 17:775–787.
6. Chuma S, et al. (2003) Mouse Tudor Repeat-1 (MTR-1) is a novel component of chromatoid bodies/nuages in male germ cells and forms a complex with snRNPs. *Mech Dev* 120:979–990.
7. Callebaut I, Mornon JP (2010) LOTUS, a new domain associated with small RNA pathways in the germline. *Bioinformatics* 26:1140–1144.
8. Anantharaman V, Zhang D, Aravind L (2010) OST-HTH: A novel predicted RNA-binding domain. *Biol Direct* 5:13.
9. Botuyan MV, et al. (2006) Structural basis for the methylation state-specific recognition of histone H4-K20 by 53BP1 and Crb2 in DNA repair. *Cell* 127:1361–1373.
10. Chuma S, et al. (2006) Tdrd1/Mtr-1, a tudor-related gene, is essential for male germ-cell differentiation and nuage/germinal granule formation in mice. *Proc Natl Acad Sci USA* 103: 15894–15899.
11. Chen C, et al. (2009) Mouse Piwi interactome identifies binding mechanism of Tdrkh Tudor domain to arginine methylated Miwi. *Proc Natl Acad Sci USA* 106:20336–20341.

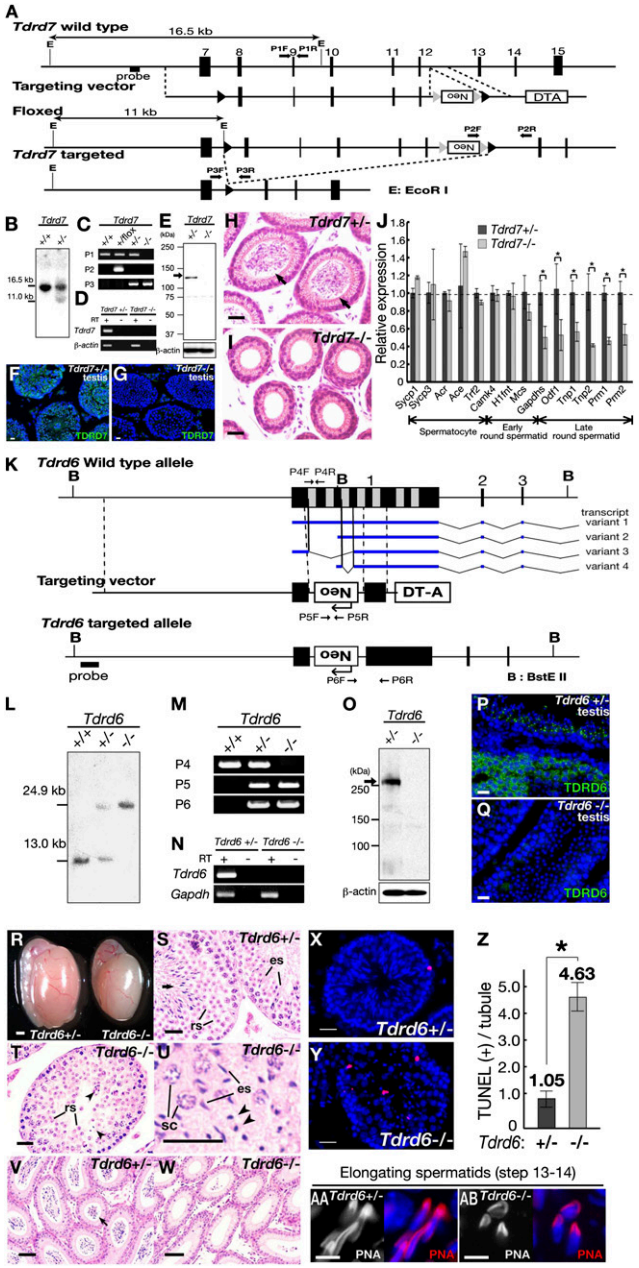

Fig. S2. Gene-targeted disruption of *Tdrd7* and *Tdrd6*. (*A*) A gene-targeting construct for *Tdrd7*. The exons are shown as filled boxes and the *loxP* and *FRT* sites as black and gray arrowheads. The resultant allele lacks exons 8–12 and is a null (see *D*–*G*). E, EcoRI. (*B* and *C*) Southern blot (*B*) and PCR (*C*) genotyping of *Tdrd7* gene-targeted mice. The probe and PCR primers are indicated in *A*. (*D*) RT-PCR of *Tdrd7*$^{+/-}$ and *Tdrd7*$^{-/-}$ testes for *Tdrd7*. Actb was used as a control. RT, reverse transcription. (*E*) Western blots of testis lysates for TDRD7 (*Upper*) and β-actin (*Lower*). The arrow indicates TDRD7. (*F* and *G*) Immunostain of *Tdrd7*$^{+/-}$ (*F*) and *Tdrd7*$^{-/-}$ (*G*) testis sections for TDRD7. TDRD7 was not detected in *G*. (*H* and *I*) H&E-stained sections of *Tdrd7*$^{+/-}$ (*H*) and *Tdrd7*$^{-/-}$ (*I*) epididymides at 2 mo of age. The arrows (*H*) indicate mature spermatozoa. (*J*) Real-time RT-PCR of *Tdrd7*$^{+/-}$ and *Tdrd7*$^{-/-}$ testes at postnatal day 24 for the expression of spermatogenesis markers. The data were normalized to β-actin and are shown as the means and SD ($n = 3$). Asterisk, $P < 0.05$. (*K*) A targeting construct for *Tdrd6*. The resultant allele lacks most of the first exon that encodes for the tudor domains (shaded boxes). The four transcript variants (blue lines) are from ref. 1. B, BstEII. (*L* and *M*) Southern blot (*L*) and PCR (*M*) genotyping of *Tdrd6* gene-targeted mice. The probe and PCR primers are indicated in *K*. (*N*) RT-PCR of *Tdrd6*$^{+/-}$ and *Tdrd6*$^{-/-}$ testes for *Tdrd6*. *Gapdh* was used as a control. (*O*) Western blots of testis lysates for TDRD6 (*Upper*) and β-actin (*Lower*) as a control. The arrow indicates TDRD6. (*P* and *Q*) Immunostain of *Tdrd6*$^{+/-}$ (*P*) and *Tdrd6*$^{-/-}$ (*Q*) testis sections for TDRD6. TDRD6 was not detected in *Q*. (*R*) The gross appearance of *Tdrd6*$^{+/-}$ and *Tdrd6*$^{-/-}$ testes at 2 mo. (*S*–*U*) H&E-stained sections of *Tdrd6*$^{+/-}$ (*S*) and *Tdrd6*$^{-/-}$ (*T* and *U*) testes at 2 mo. The arrow indicates mature spermatozoa. In *Tdrd6*$^{-/-}$ testes (*T* and *U*), elongating spermatids were observed, but were reduced in number and had aberrant nuclear morphologies (arrowheads). sc, spermatocytes, rs, round spermatids, es, elongating spermatids. (*V* and *W*) H&E-stained sections of *Tdrd6*$^{+/-}$ (*V*) and *Tdrd6*$^{-/-}$ (*W*) epididymides at 2 mo. The arrow indicates mature spermatozoa. (*X* and *Y*) TUNEL staining (red) of apoptotic cells in *Tdrd6*$^{+/-}$ (*X*) and *Tdrd6*$^{-/-}$ (*Y*) testis sections counterstained with a Hoechst dye (blue). (*Z*) Quantification of apoptotic cells in *Tdrd6*$^{+/-}$ and *Tdrd6*$^{-/-}$ testes. Apoptotic cells were counted in 50 seminiferous tubule cross-sections (the means and SE are shown). Asterisk, $P < 0.01$. (*AA* and *AB*) Acrosome staining [peanut agglutinin (PNA), red] of *Tdrd6*$^{+/-}$ (*AA*) and *Tdrd6*$^{-/-}$ (*AB*) spermatids counterstained with a Hoechst dye (blue). *Tdrd6*$^{-/-}$ spermatids (*AB*) had elongating nuclei with acrosomes spreading over (steps 13–14 spermatids). (Scale bars: *F*–*I*, *P*, *Q*, and *S*–*Y*, 25 μm; *R*, 1 mm; *AA* and *AB*, 10 μm.)

1. Hosokawa M, et al. (2007) Tudor-related proteins TDRD1/MTR-1, TDRD6 and TDRD7/TRAP: Domain composition, intracellular localization, and function in male germ cells in mice. *Dev Biol* 301:38–52.

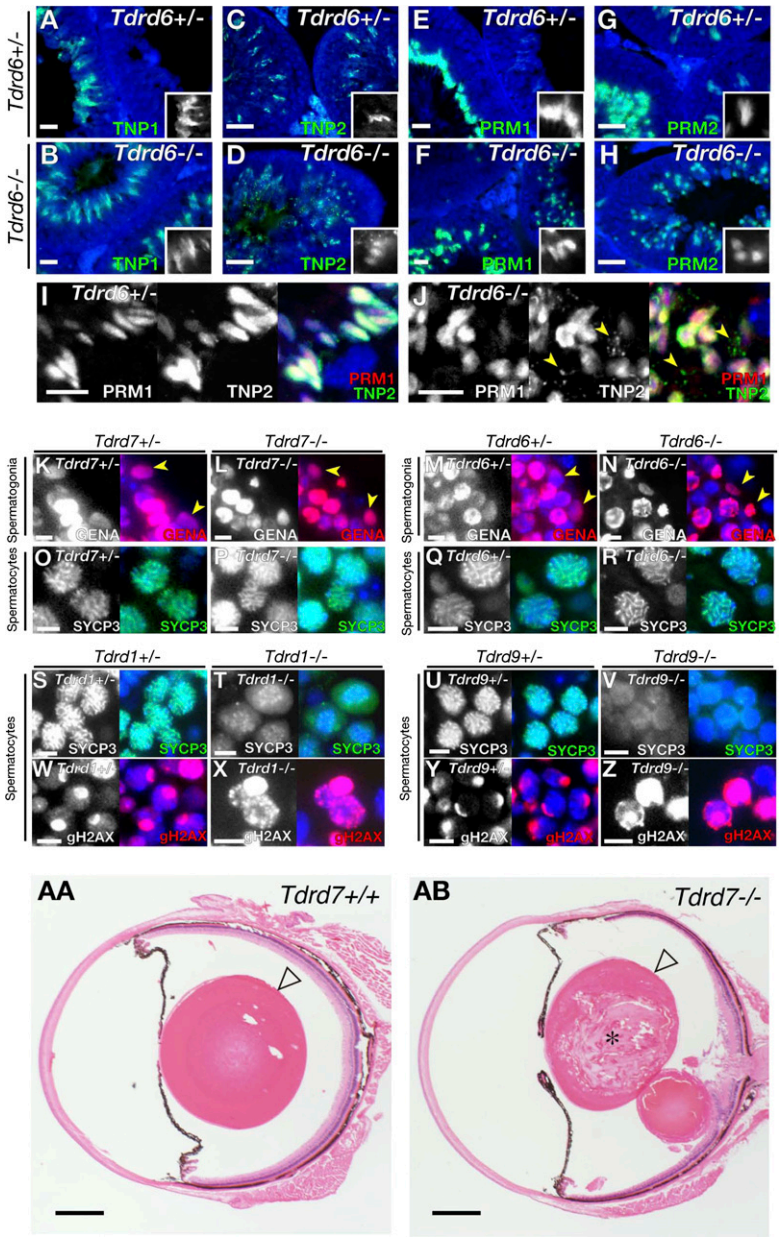

Fig. S3. *Tdrd6*$^{-/-}$ and *Tdrd7*$^{-/-}$ null phenotypes. (*A–H*) Immunostain of *Tdrd6*$^{+/-}$ (*A*, *C*, *E*, and *G*) and *Tdrd6*$^{-/-}$ (*B*, *D*, *F*, and *H*) testis sections for TNP1 (*A* and *B*), TNP2 (*C* and *D*), PRM1 (*E* and *F*), and PRM2 (*G* and *H*) counterstained with a Hoechst dye (blue). *Tdrd6*$^{-/-}$ spermatids express transition proteins and protamines. *Insets* are higher magnification views showing nuclear localization of the proteins. (*I* and *J*) Anti-PRM1 and TNP2 double immunostaining of *Tdrd6*$^{+/-}$ (*I*) and *Tdrd6*$^{-/-}$ (*J*) elongating spermatids. Note that TNP2 in *Tdrd6*$^{-/-}$ spermatids shows aberrant cytoplasmic aggregations (*J*, arrowheads) in addition to nuclear localization. (*K–N*) Immunostaining of *Tdrd7*$^{+/-}$ (*K*), *Tdrd7*$^{-/-}$ (*L*), *Tdrd6*$^{+/-}$ (*M*), and *Tdrd6*$^{-/-}$ (*N*) testis sections for germ-cell–specific nuclear antigen (GENA, red). Spermatogonia were normally seen in *Tdrd7*$^{-/-}$ and *Tdrd6*$^{-/-}$ testes (arrowheads). (*O–R*) Immunostaining of *Tdrd7*$^{+/-}$ (*O*), *Tdrd7*$^{-/-}$ (*P*), *Tdrd6*$^{+/-}$ (*Q*), and *Tdrd6*$^{-/-}$ (*R*) testis sections for SYCP3 (green). Axial elements in meiotic spermatocytes were normally observed in *Tdrd7*$^{-/-}$ and *Tdrd6*$^{-/-}$ mutants. (*S–Z*) Meiotic catastrophe of *Tdrd1*$^{-/-}$ and *Tdrd9*$^{-/-}$ mutants. *Tdrd1*$^{+/-}$ (*S* and *W*), *Tdrd1*$^{-/-}$ (*T* and *X*), *Tdrd9*$^{+/-}$ (*U* and *Y*) and *Tdrd9*$^{-/-}$ (*V* and *Z*) spermatocytes were immunostained for SYCP3 (*S–V*) or γ-H2AX (*W–Z*). In control *Tdrd1*$^{+/-}$ and *Tdrd9*$^{+/-}$ spermatocytes, meiotic synaptonemal complexes stained by SYCP3 were clearly assembled (*S* and *U*). In *Tdrd1*$^{-/-}$ (*T*) *and Tdrd9*$^{-/-}$ (*V*) mutants, such synapsis formation was severely disrupted. γ-H2AX is a marker for genome DNA double-strand breaks and was highly increased in *Tdrd1*$^{-/-}$ (*X*) and *Tdrd9*$^{-/-}$ (*Z*) spermatocytes (1, 2) compared with controls (*W* and *Y*). The nuclei were counterstained with a Hoechst dye (blue). (*AA* and *AB*) H&E-stained sections of *Tdrd7*$^{+/+}$ (*AA*) and *Tdrd7*$^{-/-}$ (*AB*) eyes (1 y). The eye lenses are indicated by open arrowheads. The region marked with an asterisk shows a cataract. There is another aberrant fiber cell mass adjoining the *Tdrd7*$^{-/-}$ lens (*AB*). (Scale bars: *A–H*, 25 μm; *I–Z*, 10 μm; *AA* and *AB*, 500 μm.)

1. Shoji M, et al. (2009) The TDRD9-MIWI2 complex is essential for piRNA-mediated retrotransposon silencing in the mouse male germline. *Dev Cell* 17:775–787.
2. Chuma S, et al. (2006) Tdrd1/Mtr-1, a tudor-related gene, is essential for male germ-cell differentiation and nuage/germinal granule formation in mice. *Proc Natl Acad Sci USA* 103: 15894–15899.

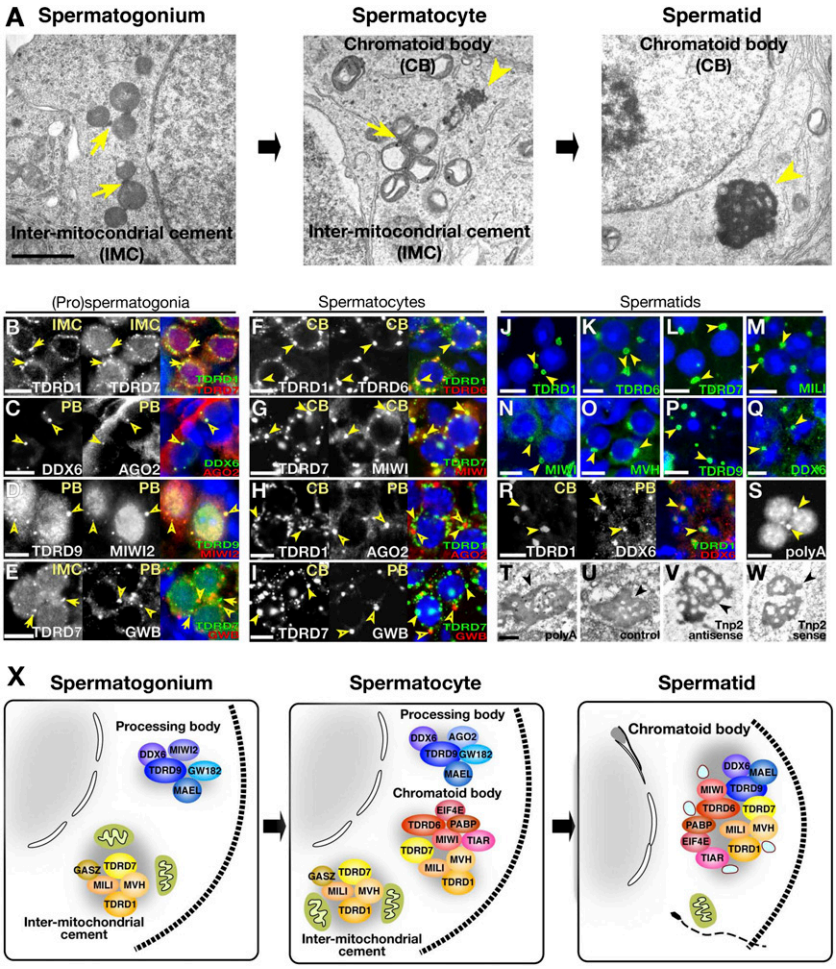

Fig. S4. Germinal granules in male germline development in mice. (*A*) Electron microscope images of germinal granules in murine male germ cells. In prospermatogonia (*Left*), intermitochondrial cement (arrows) is observed as small electron-dense material without limiting membranes among mitochondrial clusters. In meiotic spermatocytes (*Center*), the size and frequency of intermitochondrial cement increase (particularly at the pachytene stage, as shown by the arrow) compared with prospermatogonia. In the meantime, chromatoid bodies emerge independently of intermitochondrial cement and are observed as prominent, amorphous aggregates in the free cytoplasm (arrowhead). In haploid spermatids (*Right*), intermitochondrial cement is no longer seen, whereas chromatoid bodies (arrowhead) become more massive and are aggregated as a solitary architecture of submicron sizes. Chromatoid bodies at this stage occasionally show a close association with intracellular membrane vesicles. (*B–I*) Double immunostaining of fetal prospermatogonia at embryonic day 17.5 (*B–E*) and postnatal meiotic spermatocytes (*F–I*) with anti-TDRD1 and TDRD7 (markers of intermitochondrial cement and chomatoid bodies), anti-TDRD6 and MIWI (markers of chromatoid bodies), anti-DDX6, AGO2, TDRD9, MIWI2, and GWB proteins (markers of processing bodies/GW bodies) counterstained with a Hoechst dye (blue). Intermitochondrial cement, processing bodies, and chromatoid bodies are denoted by IMC, PB, and CB, respectively, and marked with arrows, open arrowheads, and arrowheads, respectively. (*J–R*) Immunostain (*J–Q*) and double immunostain (*R*) of round spermatids for chromatoid bodies. Chromatoid bodies at this stage integrate early chromatoid body proteins observed in meiotic spermatocytes (TDRD1, TDRD6, TDRD7, MILI, MIWI, and MVH) (*J–O*) with a class of processing body components (TDRD9, DDX6) (*P* and *Q*), resulting in a hybrid composition (*R*). The arrowheads indicate chromatoid bodies. (*S*) Fluorescence RNA in situ hybridization of round spermatids with an oligo(dT) probe. The arrowheads point to chromatoid bodies. (*T–W*) RNA in situ hybridization and electron microscopy of chromatoid bodies (arrowheads) for oligo(dT) (*T*), control oligo(dA) (*U*), *transition protein 2* (*Tnp2*) antisense (*V*), and control *Tnp2* sense (*W*) probes. Antisense signals (*T* and *V*, black dots) were seen at chromatoid bodies. (*X*) A summary for ribonucleoprotein (RNP) remodeling of germinal granules during male germline development. In prospermatogonia (*Left*), intermitochondrial cement and processing bodies are discrete subcellular compartments with different but related molecular compositions. In meiotic spermatocytes (*Center*), intermitochondrial cement, processing bodies, and early chromatoid bodies coexist independently of each other. Intermitochondrial cement and chromatoid bodies are structurally separate, but they share main components, whereas the latter contains additional subset of other RNP proteins (for detail, see *Results*, "Tdrd7 regulates dynamic RNP remodeling of chromatoid bodies"). Then, in postmeiotic spermatids (*Right*), intermitochondrial cement disappears, whereas chromatoid bodies greatly increase in mass and integrate processing body components, resulting in a unique hybrid architecture of germline and ubiquitous RNPs. (Scale bars: *A*, 1 μm; *B–S*, 10 μm; *T–W*, 500 nm.)

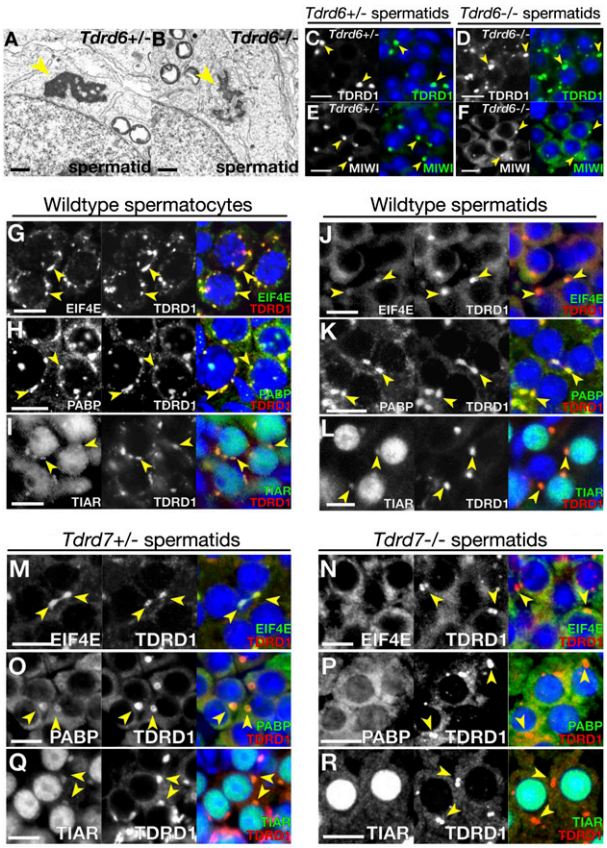

Fig. S5. (*A* and *B*) Electron microscopy of *Tdrd6*$^{+/-}$ (*A*) and *Tdrd6*$^{-/-}$ (*B*) spermatids. Chromatoid bodies (arrowheads) were fragmented and reduced in amount in *Tdrd6*$^{-/-}$ spermatids (*B*). (*C–F*) Immunostaining of *Tdrd6*$^{+/-}$ (*C* and *E*) and *Tdrd6*$^{-/-}$ (*D* and *F*) spermatids for TDRD1 (*C* and *D*) and MIWI (*E* and *F*). Nuclei were counterstained with a Hoechst dye (blue). (*G–L*) Double immunostain of meiotic spermatocytes (*G–I*) and haploid round spermatids (*J–L*) for EIF4E (*G* and *J*), PABPC1 (*H* and *K*), and TIAR (*I* and *L*), which are stress granule proteins (1, 2). Chromatoid bodies (identified with anti-TDRD1 antibody) are marked with arrowheads. (*M–R*) Double immunostain of *Tdrd7*$^{+/-}$ (*M*, *O*, and *Q*) and *Tdrd7*$^{-/-}$ (*N*, *P*, and *R*) spermatids for TDRD1 (chromatoid body marker) and EIF4E (*M* and *N*) and PABPC1 (*O* and *P*) and TIAR (*Q* and *R*). These translation regulators, which are also stress granule components, are delocalized from chromatoid bodies in *Tdrd7*$^{-/-}$ mutants. The arrowheads mark chromatoid bodies. (Scale bars: *A* and *B*, 500 nm; *C–R*, 10 μm.)

1. Kedersha NL, Gupta M, Li W, Miller I, Anderson P (1999) RNA-binding proteins TIA-1 and TIAR link the phosphorylation of eIF-2 alpha to the assembly of mammalian stress granules. *J Cell Biol* 147:1431–1442.
2. Kedersha N, et al. (2002) Evidence that ternary complex (eIF2-GTP-tRNA(i)(Met))-deficient preinitiation complexes are core constituents of mammalian stress granules. *Mol Biol Cell* 13(1):195–210.

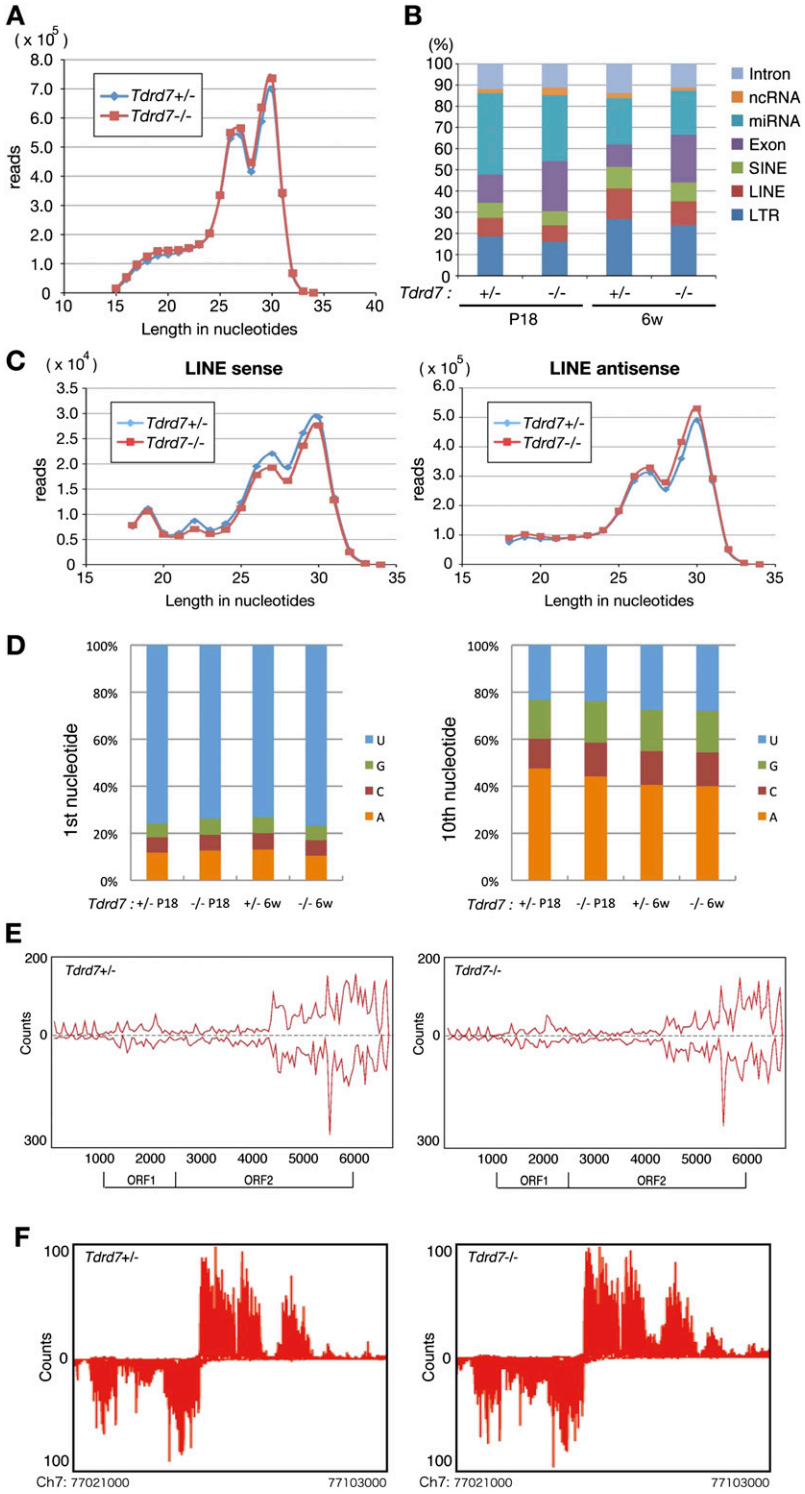

Fig. S6. *Tdrd7*$^{-/-}$ mutation does not disrupt piRNA biogenesis. Libraries of small RNA were prepared from *Tdrd7*$^{+/-}$ and control *Tdrd7*$^{-/-}$ testes at postnatal day 18 (P18) and 6 wk of age (6w) and analyzed by deep sequencing. (*A*) The size distribution of the piRNAs from each library at P18. (*B*) Genome annotation of the piRNA sequences. Retrotransposons were classified into three major groups: LTR, LINE, and SINE. (*C*) The strand orientation and length distribution of the piRNAs derived from *LINE1* retrotransposons. (*D*) The nucleotide compositions of the 1st (*Left*) and 10th (*Right*) nucleotides of the piRNA sequences. (*E*) The distribution of the piRNAs on *LINE1* consensus sequence (6 wk). (*F*) The distribution of the piRNAs on a representative genomic piRNA cluster (chromosome 7: 77021000–77103000) (6 wk).

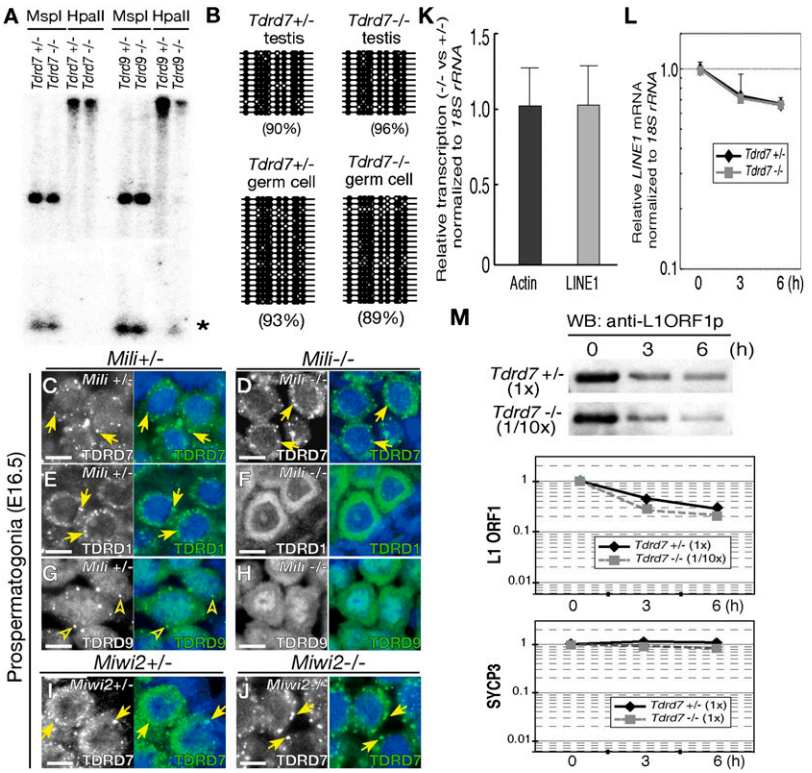

Fig. S7. (*A*) Methylation-sensitive Southern blots of genomic DNA from postnatal testes (P22) with indicated genotypes with a *LINE1* probe (type A). DNAs were digested with methylation-sensitive HpaII or its methylation-insensitive isoschizomer, MspI. The band marked with an asterisk in the HpaII lanes indicates *LINE1* hypomethylation. Demethylation was seen in the *Tdrd9*$^{-/-}$ sample (used as a control) (1), but not detectable in the *Tdrd7*$^{-/-}$ sample. (*B*) Genomic DNAs of P22 testes and FACS-purified germ cells from *Tdrd7*$^{+/-}$ and *Tdrd7*$^{-/-}$ mice were subjected to bisulfite sequencing of *LINE1* (type Tf) (2). Methylated CpG sites are shown with black circles and nonmethylated sites with open circles. Gray circles are non-CpG sites. The percentages of methylated CpGs are shown below. (*C–J*) Immunostaining of *Mili*$^{+/-}$ (*C*, *E*, and *G*), *Mili*$^{-/-}$ (*D*, *F*, and *H*), *Miwi2*$^{+/-}$ (*I*), and *Miwi2*$^{-/-}$ (*J*) embryonic testes (E16.5) for TDRD7 (*C*, *D*, *I*, and *J*), TDRD1 (*E* and *F*), and TDRD9 (*G* and *H*). The *Mili*$^{-/-}$ mutation caused TDRD1 and TDRD9 delocalization (*F* and *H*), but did not affect TDRD7 (*D*). The *Miwi2*$^{-/-}$ mutation also did not disturb TDRD7 localization (*J*) (3). Intermitochondrial cement and processing bodies are marked with arrows and open arrowheads, respectively. The nuclei were counterstained with a Hoechst dye (blue). (*K*) Relative transcription of *LINE1* measured by primary culture of testicular cells (3 wk) in the presence of uridine analog 5-ethynyluridine (EU) for 1 h. Total RNAs were extracted and then 5-EU–labeled nascent RNAs were biotinylated by click chemistry, captured on streptavidin magnetic beads, and used for cDNA synthesis followed by real-time PCR. *18S rRNA* was used for normalization. Data were obtained from four independent experiments (means and SE). (*L*) *LINE1* mRNA stability was analyzed by primary culture of testicular cells (3 wk) in the presence of 5,6-dichlorobenzimidazole, which inhibits RNA polymerase II. The cells were collected at the indicated time points (3 and 6 h), and then the relative abundance of *LINE1* mRNA normalized to *18S rRNA* was measured by real-time RT-PCR (n = 3). The vertical axis is logarithmic. (*M*) LINE1 protein stability was analyzed by primary culture of testicular cells (3 wk) in the presence of cycloheximide. The cells were collected at the indicated time points (3 and 6 h) and subjected to Western blot analyses. (*Upper* panels) Western blots for LINE ORF1. *Tdrd7*$^{-/-}$ samples were diluted at a 1:10 ratio to avoid saturation of autoradiography. The differences between *Tdrd7*$^{-/-}$ and *Tdrd7* $^{+/-}$ samples are not significant. (Scale bars: *C–J*, 10 μm.)

1. Shoji M, et al. (2009) The TDRD9-MIWI2 complex is essential for piRNA-mediated retrotransposon silencing in the mouse male germline. *Dev Cell* 17:775–787.
2. Kato Y, et al. (2007) Role of the Dnmt3 family in de novo methylation of imprinted and repetitive sequences during male germ cell development in the mouse. *Hum Mol Genet* 16: 2272–2280.
3. Carmell MA, et al. (2007) MIWI2 is essential for spermatogenesis and repression of transposons in the mouse male germline. *Dev Cell* 12:503–514.

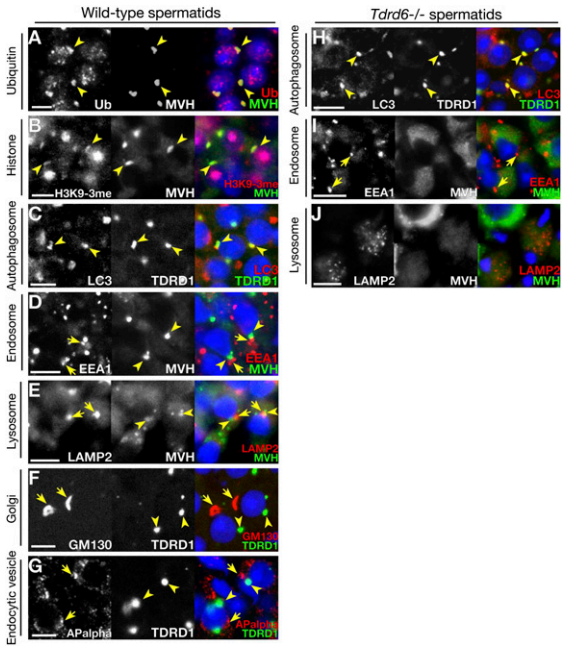

Fig. S8. Chromatoid bodies show a close spatiotemporal association with autophagosomes/lysosomes. Chromatoid bodies (*A* and *B*: MVH *Center* panels, arrowheads) at a late stage of spermatid differentiation exhibit the enrichment of ubiquitin (*A*, Ub) and the accumulation of unnecessary proteins like histones (*B*, H3K9-3me) as previously reported (1). Chromatoid bodies (*C*–*G*: TDRD1 and MVH *Center* panels, arrowheads) also show a close association with the autophagosomes (*C*, LC3), endosomes (*D*, EEA1), and lysosomes (*E*, LAMP2) during spermiogenesis. These characteristics (*A*–*E*) are hallmarks of aggresomes, the presumed function of which is to sequester unnecessary proteins and other cellular components, followed by in-cell clearance via the autophagy system. Chromatoid bodies may participate in intracellular protein turnover during spermatid morphogenesis, and in accordance, these aggresome-like features of chromatoid bodies were observed only at late stages of spermatid differentiation (after step 7), when substantial cell reconstruction takes place. Other endomembrane systems, including the Golgi apparatus (*F*, GM130, arrows) and endocytic vesicles (*G*, APα, arrows), did not show a similar correlation with chromatoid bodies (arrowheads). In *Tdrd6*$^{-/-}$ spermatids (*H*–*J*), the initial contact between chromatoid bodies and autophagosomes were seen (*H*, arrowheads), but the subsequent association of chromatoid bodies with autophagosomes/lysosomes was not observed (*I* and *J*). Chromatoid bodies were dispersed by these differentiation stages in *Tdrd6*$^{-/-}$ spermatids. Nuclei were counterstained with a Hoechst dye (blue). (Scale bars: *A*–*J*, 10 μm.)

1. Haraguchi CM, et al. (2005) Chromatoid bodies: Aggresome-like characteristics and degradation sites for organelles of spermiogenic cells. *J Histochem Cytochem* 53:455–465.

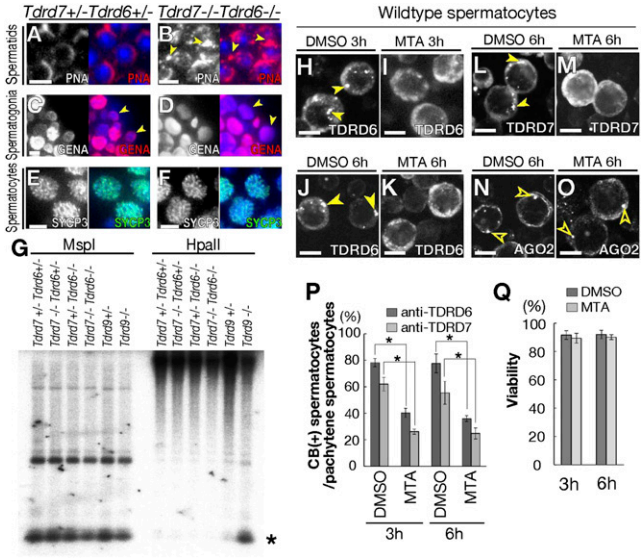

Fig. S9. (*A* and *B*) *Tdrd7*$^{+/-}$ *Tdrd6*$^{+/-}$ (*A*) and *Tdrd7*$^{-/-}$ *Tdrd6*$^{-/-}$ (*B*) spermatids stained for peanut agglutinin (PNA) (acrosome, red). In *Tdrd7*$^{-/-}$ *Tdrd6*$^{-/-}$ spermatids, acrosome formation was severely impaired (*B*, arrowheads). (*C* and *D*) Immunostaining of *Tdrd7*$^{+/-}$ *Tdrd6*$^{+/-}$ (*C*) and *Tdrd7*$^{-/-}$ *Tdrd6*$^{-/-}$ (*D*) testis sections for germ-cell–specific nuclear antigen (GENA, red). Spermatogonia (arrowheads) were normally seen in *Tdrd7*$^{-/-}$ *Tdrd6*$^{-/-}$ mutant testes (*D*) as in control *Tdrd7*$^{+/-}$ *Tdrd6*$^{+/-}$ testes (*C*). (*E* and *F*) Immunostaining of *Tdrd7*$^{+/-}$ *Tdrd6*$^{+/-}$ (*E*) and *Tdrd7*$^{-/-}$ *Tdrd6*$^{-/-}$ (*F*) testis sections for SYCP3 (green). Axial elements in meiotic spermatocytes were normally observed in *Tdrd7*$^{-/-}$ *Tdrd6*$^{-/-}$ mutant testes (*F*) as in controls (*E*). (*G*) Methylation-sensitive Southern blots of genomic DNA from postnatal day 22 testes of indicated genotypes probed with a *LINE1* probe. Genome DNAs were digested with methylation-sensitive HpaII or its methylation-insensitive isoschizomer MspI. The band marked with the asterisk on the HpaII blot indicates *LINE1* hypomethylation (seen only in the *Tdrd9*$^{-/-}$ lane, but not in the *Tdrd7*$^{-/-}$ *Tdrd6*$^{-/-}$ lane). (*H–Q*) Primary culture of wild-type testis cells. DMSO- or MTA-treated spermatocytes were immunostained for TDRD6, TDRD7 (chromatoid bodies: arrowheads, *H–M*), or AGO2 (processing bodies: open arroweads, *N* and *O*). (*P*) Quantification of spermatocytes (identified by SYCP3; $n = 150$) with chromatoid bodies (CB) (identified by using anti-TDRD6 and anti-TDRD7 antibodies). Asterisk, $P < 0.01$. (*Q*) Cell viability during the time course of primary culture as shown in *P*. Spermatocytes with normal nuclear morphologies (stained by a Hoechst dye) and SYCP3 patterns were counted ($n = 150$, means and SE). (Scale bars: *A–F* and *H–O*, 10 μm.)